Ceramics International 46 (2020) 2960–2968

Contents lists available at ScienceDirect

Ceramics International

journal homepage: www.elsevier.com/locate/ceramint

Adsorption of selected dyes on $Ti_3C_2T_x$ MXene and Al-based metal-organic framework

Byung-Moon Jun[a], Jiyong Heo[b], Nader Taheri-Qazvini[c,d], Chang Min Park[e], Yeomin Yoon[a,*]

[a] Department of Civil and Environmental Engineering, University of South Carolina, Columbia, 300 Main Street, SC, 29208, USA
[b] Department of Civil and Environmental Engineering, Korea Army Academy at Youngcheon, 495 Hogook-ro, Gokyungmeon, Youngcheon, Gyeongbuk, 38900, Republic of Korea
[c] Department of Chemical Engineering, University of South Carolina, Columbia, SC, 29208, USA
[d] Biomedical Engineering Program, University of South Carolina, Columbia, SC, 29208, USA
[e] Department of Environmental Engineering, Kyungpook National University, 80 Daehak-ro, Buk-gu, Daegu, 41566, Republic of Korea

ARTICLE INFO

Keywords:
Adsorption
Methylene blue
Acid blue 80
MXene
Metal-organic framework

ABSTRACT

MXene and metal organic framework (MOF) were used as the main adsorbents to remove synthetic dyes from model wastewater. Methylene blue (MB) and acid blue 80 (AB) were used as the model cationic and anionic synthetic dyes, respectively. To investigate the physicochemical properties of the adsorbents used, we carried out several characterizations using microscopy, powder X-ray diffraction, a porosimetry, and a zeta potential analyzer. The surface area of MXene and MOF was 9 and 630 $m^2 g^{-1}$, respectively, and their respective isoelectric points were approximately pH 3 and 9. Thus, MXene and MOF exhibited high capacity for MB (~140 $mg g^{-1}$) and AB (~200 $mg g^{-1}$) adsorption, respectively due to their electrostatic attractions when the concentrations of the adsorbents and adsorbates were 25 and 10 $mg L^{-1}$. Furthermore, the MOF was able to capture the MB due mainly to hydrophobic interactions. In terms of the advantages of each adsorbent according to our experimental results, MXene exhibited fast kinetics and high selectivity. Meanwhile, the MOF had a high adsorption capacity for both MB and AB. The adsorption mechanisms of both adsorbents for the removal of MB and AB were clearly explained by the results of our analyses of solution pH, ionic strength, and the presence of divalent cation, anion, or humic acids, as well as other characterizations (*i.e.*, Fourier-transform infrared spectroscopy and X-ray photoelectron spectroscopy). According to our results, MOF and MXene can be used as economical treatments for wastewater containing organic pollutants regardless of charge (*e.g.*, MB and AB), and positively charged one (*e.g.*, MB), respectively.

1. Introduction

Synthetic dyes have generally been used in the paper/textile industries and for beauty/drug treatments [1]. To date, over 100,000 types of synthetic dyes have been produced, and 0.7 million ton $year^{-1}$ dyestuffs are discharged into water bodies [2]. This is due to the development of the dye industry, propelled population growth [2]. One important intrinsic property of synthetic dyes is their complex chemical structure, which makes them difficult for microorganisms to degrade [3]. The presence of synthetic dyes in wastewater would affect negative aspects on ecosystems, as follows [2,4]: (i) synthetic dyes are known as toxic and carcinogenic to the living organisms near to natural water sources, (ii) it could be difficult for sunlight to penetrate natural water containing synthetic dyes, inhibiting the photosynthesis of plants, and (iii) colored wastewater containing synthetic dyes could destroy ecosystems due to the decrease in amount of oxygen dissolved in the water. Thus, the treatment of wastewater containing dyes is currently one of the most pressing environmental issues [2,5].

There are many strategies for treating wastewater containing synthetic dyes, as follows: photocatalytic removal using visible light [6], reduction by zero-valent metals [7], biodegradation [8], ozonation [9], sonocatalytic degradation [10], photo-assisted Fenton processes [11], and membrane processes [12]. However, these techniques have many weaknesses, such as high cost, undesirable byproducts, and relatively low removal rates [4]. Adsorption processes constitute an alternative method, and are characterized by higher removal rates, easy operation, good reusability, and relatively low cost for treating synthetic dyes in aqueous solution [2]. During the past few decades, many adsorbents have been used for treating wastewater (including synthetic dyes), as follows: Australian natural zeolite [13], orange peel from orange trees

* Corresponding author.
E-mail address: yoony@cec.sc.edu (Y. Yoon).

https://doi.org/10.1016/j.ceramint.2019.09.293
Received 25 July 2019; Received in revised form 5 September 2019; Accepted 30 September 2019
Available online 02 October 2019

[14], pyrolysis residues from oil shale [15], molecular sieves [16], bentonite clay [17], and activated carbon [18], metal-organic frameworks (MOFs [19]), and MXene [20]. The development of efficient adsorbents is a key factor for improving the removal efficiency of adsorption processes.

MOFs are nanoporous materials containing metal ions connected by organic ligands [19]. These materials have unique intrinsic properties, such as large pore size and crystalline structure, good thermal-resistance, large surface area, tailorable molecules, and tunable pore structure [4,21]. Thus, MOFs can be used for adsorption processes in environmental applications due to their excellent physical properties (*i.e.*, high surface area and porosity) [1]. For example, a previous study utilized Al-based MOF (*i.e.*, MIL-53(Al)) as the adsorbent for synthetic dyes, based on its outstanding physical properties [1].

Subsequently, MXene, as a nanomaterial, has also attracted much attention due to its potential environmental applications [22]. This material represents a new family of transition-metal based two dimensional materials, which are similar in structure to graphene [23]. MXene is produced by etching a layer of 'A' from a 'MAX' precursor, where M is a transition-metal, A is an IVA/IIIA element (*e.g.*, Al, Sn, Si, and *etc*), and X is nitrogen or carbon [24]. MXene can be used as an adsorbent to remove organic pollutants because of its physicochemical properties, as follows: high theoretical surface area, chemical stability, metallic conductivity, hydrophilicity, fine structure, and tunable chemistry [22]. For example, $Ti_3C_2T_x$ MXene can be applied to dye adsorption, considering its unique structure and diverse chemistries [22]. However, to the best of our knowledge, there no previous reports have comprehensively compared MOF and MXene for the treatment of wastewater containing synthetic dyes.

The main purpose of this study is to undertake a systematic investigation of the adsorption mechanisms of MOF and MXene using Fourier-transform infrared spectroscopy (FTIR) and X-ray photoelectron spectroscopy (XPS). Specifically, we evaluated the adsorption performance of dyes while varying a variety of experimental conditions, such as the adsorbent dosage, exposure time, initial concentration of adsorbates, solution temperature, solution pH, ionic strength, and presence of divalent cations, anions, or humic acids (HAs) in the dye solution. Finally, we carried out reusability tests (four cycles) of the used adsorbents to determine their practical feasibility.

2. Materials and methods

2.1. Chemicals

Analytical grade methylene blue (MB), acid blue 80 (AB), Basolite A100 MOF (*i.e.*, MIL-53(Al)), HA, HCl, NaOH, NaCl, $CaCl_2$, and Na_2SO_4 were purchased from Sigma-Aldrich (St. Louis, MO, USA). $Ti_3C_2T_x$-based MXene was obtained from Advanced Materials Development Expert Store (Hangzhou, Zhejiang, China). MB and AB were used as representative cationic and anionic synthetic dyes, respectively. Table S1 summarizes the physicochemical properties of target dyes (*i.e.,* MB and AB). Furthermore, Al-based A100 MOF and $Ti_3C_2T_x$-based MXene were used as the main adsorbents in this study. All of the experimental solutions were prepared using ultrapure deionized (DI) water.

2.2. Characterizations

Several characterizations were performed to determine the physicochemical properties of each adsorbent. The surface morphology of the adsorbents was measured using scanning electron microscopy (SEM; S-4200; Hitachi, Tokyo, Japan) and transmission electron microscopy (TEM; Titan G2; FEI, OR, USA) to obtain low and high resolution images, respectively [25,26]. The crystallinity of each adsorbent was analyzed by powder X-ray diffraction (PXRD; D/max-2500; Rigaku, Tokyo, Japan) [27]. The surface area of each adsorbent was measured by a porosimetry (Quadrasorb SI; Quantachrome, Boynton Beach, FL, USA) using N_2 adsorption and desorption isotherms, as in a previous study [21]. We measured the surface charge using a zeta potential analyzer (ZetaPals; Brookhaven Instruments Corporation, Holtsville, NY, USA) at pH values of 3, 5, 7, 9, and 11. The pH of the solution was adjusted by 1 M HCl or NaOH. We analyzed the chemical bonds and elements of the adsorbents using Fourier transform infrared spectroscopy (FTIR; Thermo Nicolet; Madison, WI, USA) and XPS (PHI Quantera SXM; ULVAC-PHI, Inc., Osaka, Japan), respectively [28,29], between pristine adsorbents and adsorbate-adsorbed adsorbents.

2.3. Adsorption and reusability tests

Adsorption tests were conducted in a 50 mL Falcon tube, with a total volume of 40 mL, 10 mg L^{-1} of adsorbate, and 100 mg L^{-1} of adsorbents for the basic experimental conditions. Specific adsorption tests under the following experimental conditions: (i) dosage of adsorbents, 25, 50, 75, or 100 mg L^{-1}, (ii) contact time, 0–24 h, (iii) initial concentration of adsorbates, 5, 7.5, 10, 20, or 40 mg L^{-1}, (iv) solution temperature, 293, 303, or 313 K, (v) solution pH, 3.5, 7, or 9.5, (vi) concentration of HA, 2.5 or 10 mg L^{-1}, and (vii) background ions, 300 μS/cm NaCl, 300 μS/cm $CaCl_2$, 300 μS/cm Na_2SO_4, 600 μS/cm NaCl, or 300 μS/cm NaCl. The electrolyte concentrations were measured using a calibrated conductivity meter [28,30]. Solution samples containing adsorbents after the experiments were filtered using a 0.2 μm syringe filter to measure the adsorbate concentrations. The concentration of each adsorbate was obtained using a UV–Vis spectrophotometer (Agilent Technologies, Santa Clara, CA, USA), following our previous study [20]. All of our experimental results were averaged based on two independent tests.

The desorption of the adsorbates from MXene was investigated using 0.1 M HCl for 4 h, followed by 0.1 M NaOH for 4 h, following previous studies [31,32]. In the case of MOF, we used acetone containing 0.1 M HCl as a cleaning solution, for 8 h, based on another study [33]. After the cleaning process, the adsorbents were filtered with a membrane with 0.2-μm pores, and then rinsed using DI water. The washed adsorbents were stored in an oven until the further adsorption test.

2.4. Results analysis

The removal rate (R) of adsorbates by adsorbents were calculated by Eq. (1) [34,35].

$$R\,(\%) = 1 - \frac{C_e}{C_0} \times 100 \tag{1}$$

where C_e and C_0 (mg L^{-1}) are the concentration of dyes in equilibrium and initial state, respectively.

The adsorption capacity (q_t, mg g^{-1}) and equilibrium adsorption capacity (q_e, mg g^{-1}) of each adsorbents were calculated by Eqs. (2) and (3), respectively.

$$q_t = \frac{(C_0 - C_t)V}{m} \tag{2}$$

$$q_e = \frac{(C_0 - C_e)V}{m} \tag{3}$$

where C_t (mg L^{-1}) is the concentration of dye at the contact time, V (L) is the volume of dye solution, and m (g) is the adsorbent dosage. Based on a previous study [27], we analyzed the results obtained from Eqs. (2) and (3), and investigated the kinetic and isotherm properties of the specimens using pseudo-first and second order, Elovich, and intraparticle diffusion kinetic models, with Langmuir and Freundlich equations used as isotherm models.

3. Results and discussion

3.1. Characterization of the adsorbents

We used SEM and TEM images to determine the surface morphology of the adsorbents; Fig. S1 (a.1) and (b.1) is representative microscopic images of MXene and MOF, respectively. We confirmed the accordion-like surface microstructure of MXene and spherical MOF particles in the SEM and TEM images, which showed similar patterns to those reported previously [1,36]. Furthermore, the crystallinity of each adsorbent was analyzed by PXRD as shown in Fig. S1 (a.2) and (b.2). The major peaks of each adsorbent were in good agreement with previously reported studies [20,36]. Fig. S1 (a.3) and (b.3) shows the surface area of each adsorbent, which we measured using a porosimetry, based on N_2 adsorption and desorption isotherms. According to these results, the surface area of MXene and MOF was approximately 9 and 630 $m^2 g^{-1}$, respectively. Hence, MOF has a much higher surface area than MXene. In other words, MOF can achieve better q_e for organic pollutants due to the van der Waals force if there is no specific adsorption mechanism [37]. These adsorbent surface areas agree with others reported in the literature (*i.e.*, ~13 $m^2 g^{-1}$ for MXene [38] and ~500 $m^2 g^{-1}$ for MOF [39]). The surface charges of the adsorbents at pH 3, 5, 7, 9, and 11 were evaluated using a zeta potential analyzer, as shown in Fig. S1 (a.4) and (b.4); the points of zero charge (pH_{pzc}) of MXene and MOF were approximately 3 and 9, respectively. These charge characteristics are comparable to those of previous studies [40,41]. Based on these results, MXene and MOFs could by electrostatically attracted to positively and negatively charged adsorbates, respectively, at neutral pH values.

3.2. Adsorption of dyes: study of dosage, kinetics, and isotherms

3.2.1. Dosage of MXene and MOF

The adsorbent dosage is among the factors determining q_e, so we investigated the effects of dosage on dye adsorption performance using MXene and MOF, as described in Fig. S2 (a) and (b), respectively. The removal rate and q_e of dyes increased and decreased continuously, respectively, as the dosages of both adsorbents increased (Fig. S2 (a) and (b)). The opposite tendency for the removal rate and q_e was may resulted from the relative difference between the concentration of adsorbates and number of adsorption sites [42]. In other words, fewer occupied adsorbent sites leads to greater adsorption due to the relatively higher diffusion rate [27]. In terms of the adsorption performance for each dye, MXene and MOF achieved better removal rates of MB and AB, respectively. This can be explained by electrostatic interactions due to the opposite charges between the adsorbates and adsorbents, as mentioned in Section 3.1. The specific adsorption mechanisms of both dyes by MXene and MOF are discussed in Section 3.4, based on FTIR and XPS measurements. The maximum dosages of MXene and MOF (100 mg L^{-1}) were selected as the optimal amounts of adsorbents for further study of water chemistry factors, as they achieved the highest removal rates of both dyes.

3.2.2. Kinetics study

We studied the kinetics of MXene and MOF to evaluate the effect of exposure time on MB and AB adsorption; Fig. 1 (a) and (b) shows the adsorption performance of MB and AB, respectively. These results are consistent with the adsorbent dosages (Section 3.2.1), because MXene and MOF achieved better removal rates of MB and AB, respectively. Since interestingly, the adsorption of MB by MXene became saturated within 30 min, in particular, fast adsorption of positive charged organic pollutant may be one of the advantages of using MXene as an adsorbent. Subsequently, MOF achieved an AB removal rate of over 80% within 120 min, and its q_e value was slightly higher than that of MXene for removing MB; thus, a high q_e may be one of the advantages of using MOF as an adsorbent. Furthermore, MOF achieved a removal rate of MB of approximately 40%, whereas MXene did not remove AB. Thus, based on the results of our kinetic study, shown in Fig. 1 (a) and (b), the adsorption mechanisms of MB and AB should differ. Furthermore, Fig. 1 (c)–(f) shows the four different kinetic models obtained using the q_e data displayed in Fig. 1 (a) and (b), and we summarize the kinetic parameters of dye adsorption by MXene and MOF in Table S2. Both adsorbents were well characterized by the pseudo-second order kinetic model, and these results are similar to those of other related studies [11,12,27,32,38,43], where MXene and MOF were used as adsorbents for treating organic/inorganic pollutants.

3.2.3. Isotherm study

We carried out an isotherm study while varying the initial concentration of the adsorbate (Fig. S3). The removal rates and q_e of the dyes increased and decreased monotonically, respectively, with increasing dosages of both MXene (Fig. S3 (a.1)) and MOF (Fig. S3 (a.2)). This pattern is consistent with the results of Section 3.2.1, so the number of adsorption sites with respect to the concentration of adsorbates is a critical factor determining the adsorption performance. To investigate this mechanism in terms of the adsorption isotherms of MXene and MOF for MB and AB, we applied two different isotherm models in this study. Langmuir and Freundlich isotherm models are known as monolayer and multilayer adsorption models, respectively [12,27]. Fig. S3 (b.1) and (c.1) shows MB removal by MXene using the Langmuir and Freundlich models, respectively. The MXene adsorption was well explained by the Freundlich model, as indicated by its higher R^2 value. The MOF adsorption agreed well with the results predicted by the Langmuir model in the cases of both MB and AB removal, as shown in Fig. S3 (b.2) and (c.2), respectively. These different tendencies may be due to their different intrinsic properties, and are in good agreement with previous studies [1,11,12,20,38] reporting isotherms of MXene and MOF for the removal of organic/inorganic pollutants.

3.3. Influence of water chemistry factors on dye adsorption

3.3.1. Solution temperature

To evaluate the effects of solution temperature on the adsorption performance, we carried out dye adsorption experiments with MXene (Fig. 2 (a)) and MOF (Fig. 3 (a)) at temperatures of 293, 303, and 313 K. The removal rate and q_e values of the dyes improved as the solution temperature increased, for both adsorbents. Based on q_e and the Gibbs equation reported in a previous study [27], we obtained thermodynamic parameters to explain the influence of solution temperature on the rates of dye removal by the adsorbents (Table S3). Both adsorbents had spontaneous reactions due to the negative value of ΔG, so increasing the solution temperature enhanced the dye adsorption properties of both MXene and MOF. Furthermore, Table S3 shows that adsorption was an endothermic process (*i.e.*, $\Delta H > 0$) with increasing randomness (*i.e.*, $\Delta S > 0$) when MOF and MXene adsorbed MB and AB. Thus, the solution temperature is also an important factor affecting the adsorption performance.

3.3.2. Solution pH

The surface charge of the adsorbents depends on the solution pH, so this factor should be considered for practical purposes [12,38]. Figs. 2 (b) and 3 (b) shows the effects of the solution pH on the removal rate and q_e of dyes when MXene and MOF were used as adsorbents, respectively. In Fig. 2 (b), it can be seen that the removal rate and q_e of MB by MXene increased with increasing solution pH. This may be due to electrostatic interactions, based on both pK_a of MB (Table S1) and the isoelectric point of MXene (Fig. S1 (a.4)). However, MXene was not able to remove AB due to electrostatic repulsion. Subsequently, the removal rate of AB by MOF was higher than that of MB under acid (*i.e.*, pH 3.5) and neutral (*i.e.*, pH 7) conditions. However, we observed opposite trends under standard (*i.e.*, pH 9.5) conditions. This indicates that electrostatic effects are the dominant mechanism governing interactions between dyes and MOF, based on the pK_a of MB and AB (Table S1)

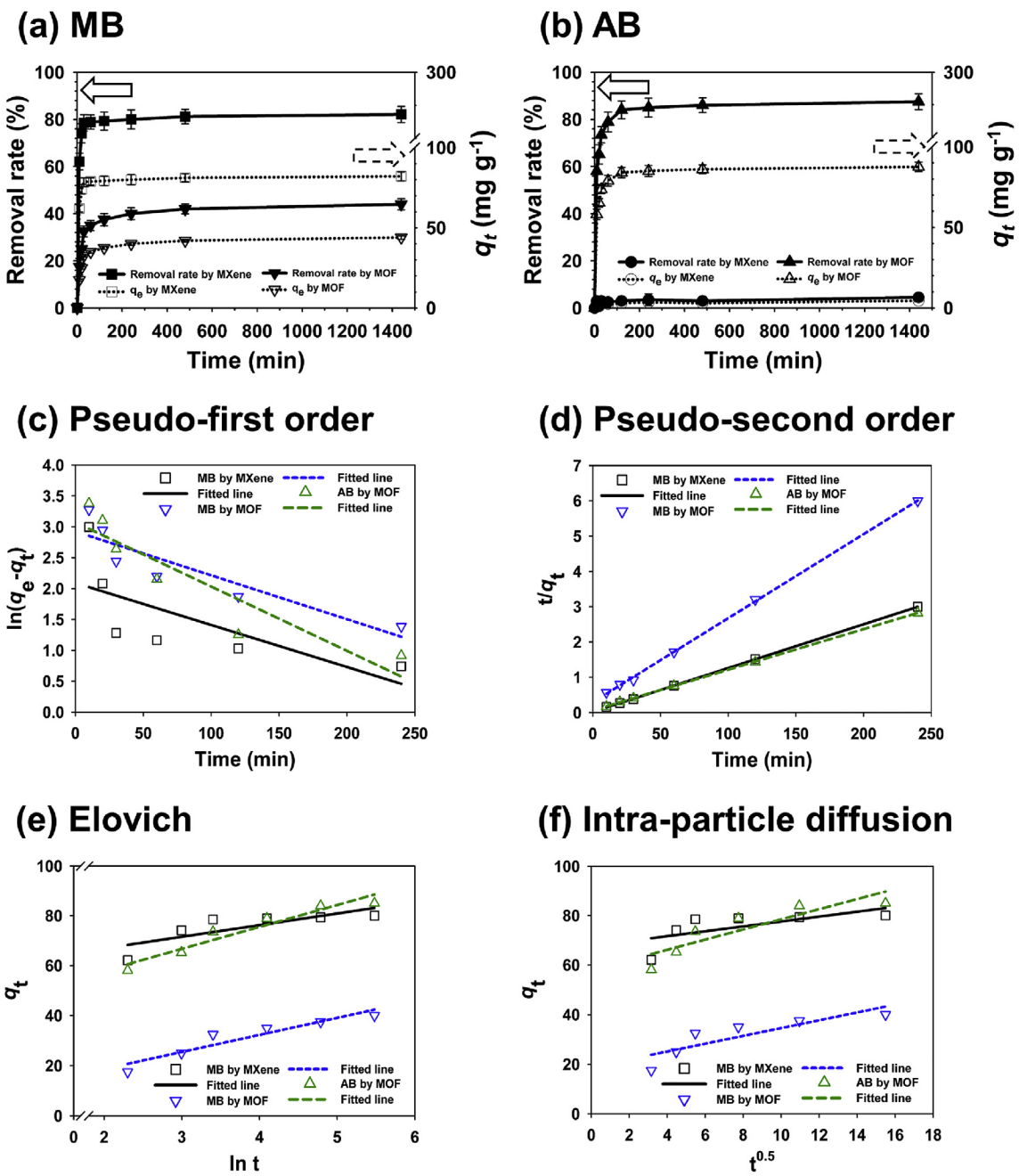

Fig. 1. Adsorption kinetic study of (a) MB and (b) AB dyes depending on contact time. Linear fitting lines of adsorption of dyes by each adsorbents through (c) pseudo-first-order, (d) pseudo-second-order, (e) Elovich, and (f) intra-particle diffusion kinetic model.

and isoelectric point of MOF (Fig. S1 (b.4)). Meanwhile, the higher removal rate of AB than MB by MOF under neutral pH values can be explained by a supplementary hydrogen bonding effect, considering the hydrogen donors (*i.e.*, H elements of amine groups) of AB and hydrogen acceptors (*i.e.*, O elements of organic linker) of MOF. However, the main adsorption mechanism of dyes by MOF was electrostatic interaction, based on the overall trends. Thus, electrostatic interaction was the most critical factor determining the adsorption performance of both adsorbents.

3.3.3. Background ions

Ionic strength and divalent cations/anions affect adsorption performance when electrostatic interaction is the main adsorption mechanism [27]. Thus, we considered the effect of background ions on dye adsorption by the adsorbents, based on previous experimental conditions [27,44,45]. Figs. 2 (c) and 3 (c) shows the effects of background ions on the removal rate and q_e of dyes when MXene and MOF were used as the adsorbent, respectively. At first, increasing ionic strength (*i.e.*, from NaCl 300 to 1,200 μS/cm) led to a decrease in the removal rate and q_e of MB by MXene (Fig. 2 (c)) and AB by MOF (Fig. 3 (c)). These results may be explained by the screening effects of the adsorbents arising from the change in the electrical double layer generated by the increased ionic strength [46]. In other words, high ionic strength in the solution weakened the electrostatic interactions between the adsorbents and adsorbates. Furthermore, increased ionic strength slightly increased the removal rate and q_e of MB by MOF (Fig. 3 (c)), which may have been due to weakened electrostatic repulsion between the MB and MOF. Subsequently, divalent cations and anions in the solution will also have affected the removal rate and q_e of the dyes, as shown in Figs. 2 (c) and 3 (c). Both adsorbents showed that divalent

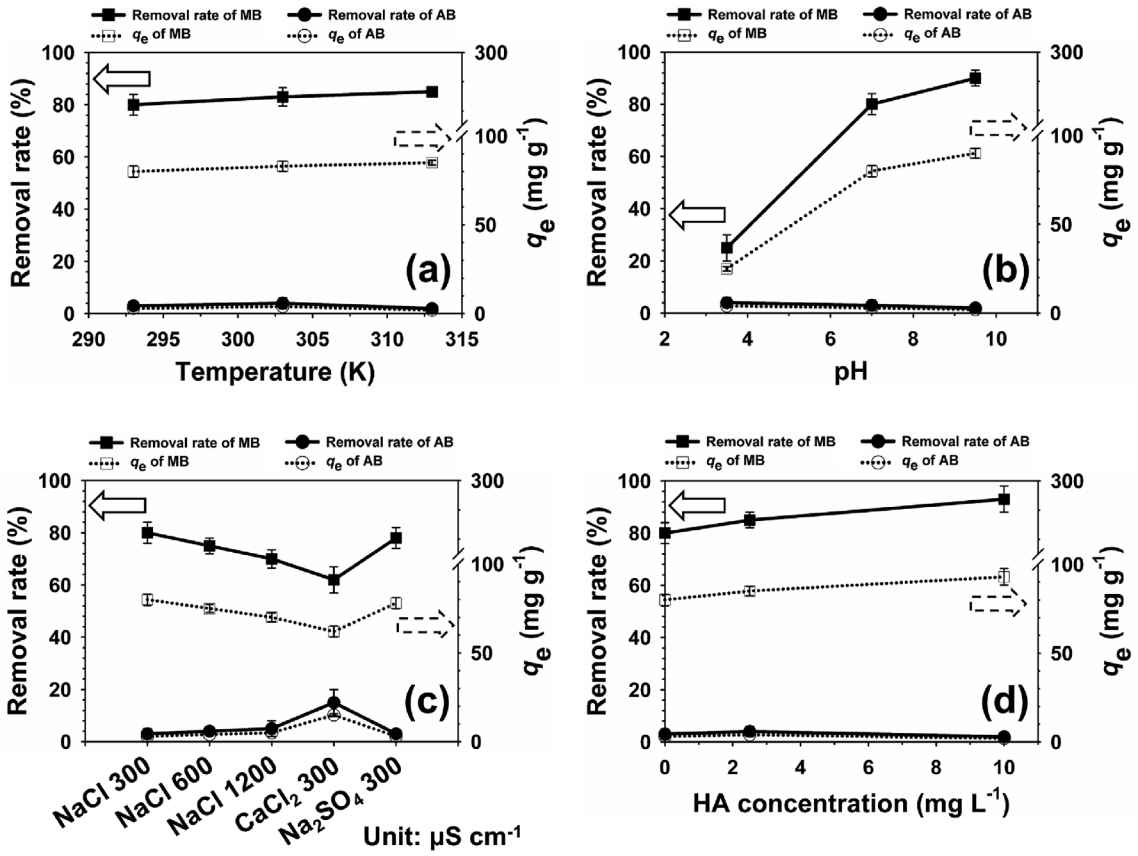

Fig. 2. Effect of (a) solution temperature, (b) solution pH, (c) background ions, and (d) existence of HA on the removal rate and q_e of dyes when MXene was used as adsorbent.

counter-ions for dyes enhanced the removal rate and q_e of the dyes. For example, the adsorption performance of AB by MOF was improved when Ca^{2+} was present in the solution, as shown in Fig. 3 (c). However, the existence of divalent co-ions in dyes decreased adsorption performance due to competition between co-ions and dyes. The results of our analysis of background ion effects support our hypothesis that electrostatic interaction is the main adsorption mechanism in this study.

3.3.4. Humic acids

According to previous studies, the presence of HA in solution affects the removal rate and q_e of the adsorbate, so we evaluated adsorption performance after adding 2.5 and 10 mg L^{-1} HA to the solution, based on methods used in previous studies [27,45]. Because HA consists of carboxylic acids and aromatic rings [47], it may act as a multivalent anion, like SO_4^{2-}, as mentioned in Section 3.3.3. Figs. 2 (d) and 3 (d) show the effect of HA on the removal rate and q_e of dyes when MXene and MOF were used as adsorbents, respectively. The results were similar to those obtained when divalent anions were added to the solution, as shown in Figs. 2 (c) and 3 (c). Interestingly, the decrease in the removal rate of AB by MOF was smaller than the increase in the removal rate of MB by MOF (Fig. 3 (d)). Thus, there is an additional adsorption mechanism in the case of MOF. One plausible reason for this result could be the hydrophobic interactions between aromatic rings, considering the chemical structures of MOF and HA. This phenomenon was also observed when MOF was used as an adsorbent for pharmaceutical pollutants (*i.e.*, carbamazepine) [48]. The relationship between the adsorption mechanism and experimental results will be discussed in the context of FTIR and XPS results in Section 3.4.

3.4. Plausible adsorption mechanism of dyes

Herein, we analyze the chemical bonds and elemental composition of pristine adsorbents and adsorbates-adsorbed adsorbents, to clarify the potential dye adsorption mechanisms. Initially, the difference between pristine adsorbents and adsorbates-adsorbed adsorbents was confirmed by FTIR, used to characterize the chemical bonds. As shown in the FTIR peaks of Fig. S4, MB and AB powder contain intrinsic peaks at 1,593/879 and 1,060 cm^{-1} due to C=N/N_{het}···HO and SO_3^-, respectively [2,3]. Hence, new peaks at 1,593/879 cm^{-1} appeared in the cases of both MXene and MOF after reaction with MB. However, we only detected a new peak at 1,060 cm^{-1} in the case of MOFs after reacting with AB. These results, which suggest that MXene is not able to trap AB in aqueous solution due to its electrostatic repulsion effect, are in good agreement with those described in Sections 3.2 and 3.3. Second, the differences between the pristine adsorbents and adsorbates-adsorbed adsorbents, in terms of chemical elements, were investigated based on XPS measurements. According to XPS measurement (Fig. 4 (a)), the composition of MXene consists of Na, C, Ti, F, and O elements. Meanwhile, the composition of MOF consists of Al, C, and O elements. Fig. 4 (a) shows wide XPS spectra of adsorbents and adsorbates, and the blue circle in Fig. 4 (a) represents the absence of an N peak in the case of reactions between MXene and AB. These results are in agreement with those of the FTIR peaks shown in Fig. S4.

Specifically, Fig. 4 (b) and (c) shows the N 1s peaks of MXene and MOF when they reacted with MB and AB, respectively. There were differences in the N 1s peaks for MB between MXene and MOF (Fig. 4(b)); some of the MXene N 1s peak shifted to a lower binding energy, which may be due to the negative charge of MXene being strongly bonded to the positive charge of MB. Thus, based on the peak shift in Fig. 4(b), MXene captured MB electrostatically. This

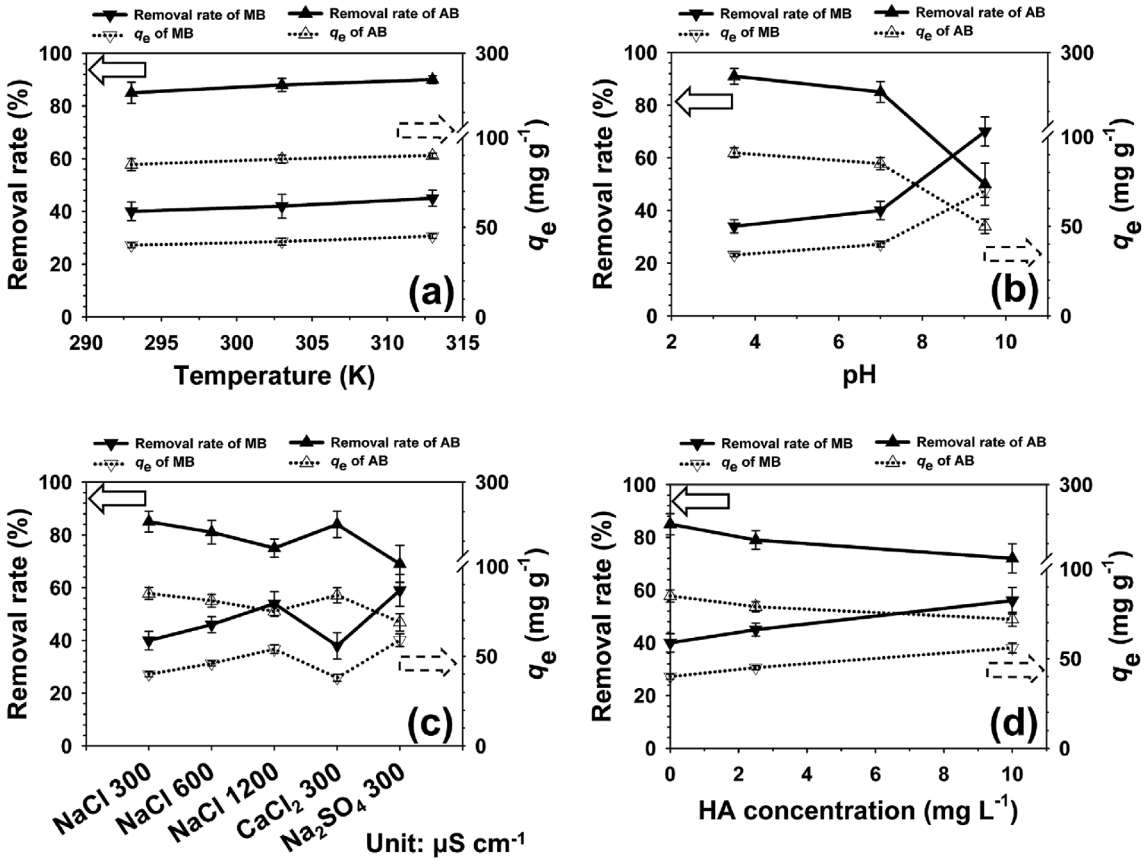

Fig. 3. Effect of (a) solution temperature, (b) solution pH, (c) background ions, and (d) existence of HA on the removal rate and q_e of dyes when MOF was used as adsorbent.

phenomenon is supported by the Na 1s, Ti 2p, and O 1s peaks shown in Fig. S5 (a), (b), and (c), respectively. The Na 1s peak decreased after reacting with MB (Fig. S5 (a)), which may be due to the ion-exchange effect between Na^+ and MB, considering previously reported results [43]. In the case of Ti 2p, as shown in Fig. S5 (b), Ti 2p was shifted to a higher binding energy due to the strong binding effect between Ti-O and MB [43]. Furthermore, the O 1s peak could be deconvoluted by [Ti-O]$^-$ and Ti-OH at 530.0 and 532.0 eV, respectively (Fig. S5 (c), and the area of the Ti-OH peak decreased after reacting with MB due to the surface complexation [43].

In the same way, the MOF adsorption mechanism could be explained by the XPS peaks shown in Fig. S5 (d), (e), and (f), which represent the XPS spectra of Al 2p, O 1s, and C 1s peaks, respectively, of pristine and MB- or AB-adsorbed MOFs. In other words, the Al 2p and O 1s peaks were shifted to a higher binding energy in the case of reactions with AB (Fig. S5 (d) and (e)), and these results verify that MOF was able to capture AB due to electrostatic interactions. Furthermore, the deconvoluted C=C peaks in the MOF were shifted slightly to a higher binding energy in both cases (*i.e.*, reaction with AB and MB), as shown in Fig. S5 (f). This could be resulted from the hydrophobic interactions between aromatic rings [49]. Thus, MOF could adsorb MB, the charge of which is opposite to that of MOF, arising from hydrophobic interactions. Fig. 5 shows a plausible schematic diagram of the adsorption mechanisms of dyes by MXene and MOF, based on the FTIR/XPS results presented in Section 3.4 and performance tests related to the water chemistry factors discussed in Section 3.3.

3.5. Regeneration of used adsorbents

The regeneration of used adsorbents is a critical factor determining practical feasibility [50]. In this study, we analyzed the removal of MB by MXene, and of AB by MOF, in the regeneration tests; the higher q_e was considered in each case, as shown in Section 3.2 and 3.3. Fig. 6 shows the reusability of MXene for AB removal after four cycles, for MB and MOF. Both adsorbents had slightly lower removal rates after four cycles; this may be due to the imperfect recovery of adsorbents using physical separation, because the N 1s peak of MXene and MOF disappeared completely after washing, as shown in Fig. 4 (b) and (c). Both adsorbents still had a q_e higher than 50 mg g^{-1} after four cycles of reuse, so both adsorbents can be used as economical and practical adsorbents for treating wastewater containing dyes.

4. Conclusions

Herein, we comprehensively characterized MXene and MOF by microscopy (*i.e.*, SEM and TEM), XRD, porosimetry, and zeta potential analysis. Furthermore, this study aimed to investigate the feasibility of MXene and MOF for the treatment of wastewater containing synthetic dyes (*i.e.*, MB and AB), so these materials were systematically studied to determine meaningful water chemistry factors. MXene and MOF had isoelectric points at pH values of approximately 3 and 9, respectively, based on the results of the zeta potential analysis. According to their intrinsic properties, MB and AB had positive and negative charges, respectively. Thus, for MB dye, MXene achieved a better q_e than MOF in a short time (~30 min). On the other hand, MOF achieved a better q_e in the case of AB, based on the q_e at different solution pH values. Electrostatic interaction was the main adsorption mechanism of dyes by both adsorbents, according to our experimental results using different background ions. These results were clearly explained by our FTIR and XPS measurements. Meanwhile, even though MOF had a positive charge at neutral pH values, it was able to capture MB in aqueous solution due to hydrophobic interactions. This conclusion was also

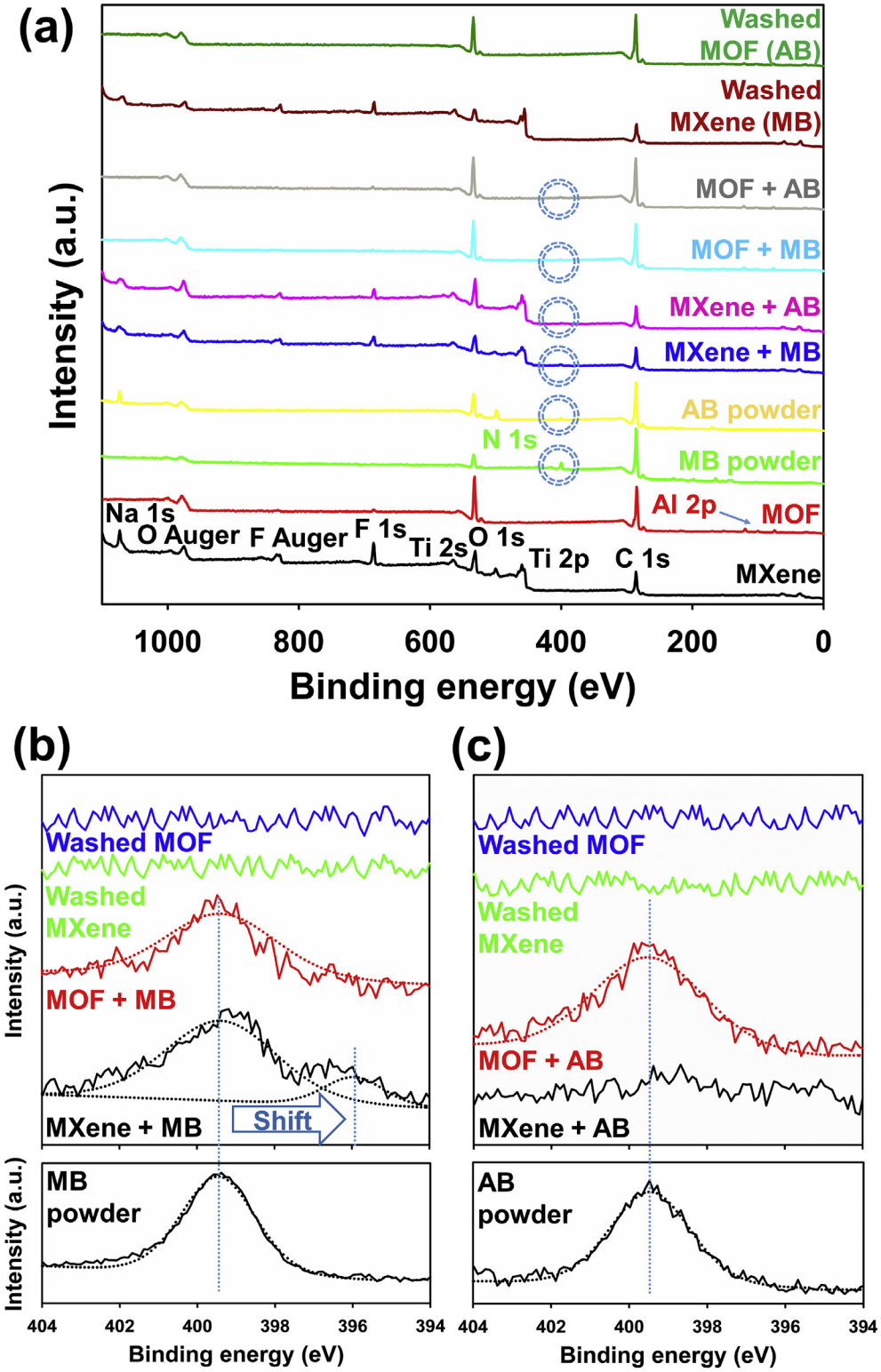

Fig. 4. XPS spectra of (a) wide scan of adsorbents and adsorbates, (b) N 1s of MB adsorbed and washed adsorbents, and (c) N 1s of AB adsorbed and washed adsorbents.

supported by our experimental results obtained under different concentrations of HA, as well as by the XPS study. The adsorption performance of MXene and MOF was evaluated using the Freundlich and Langmuir isotherm models, respectively. The behavior of both adsorbents was in good agreement with the pseudo-second-order kinetic model. Finally, both adsorbents had good reusability, so MXene and MOF are economical and practical adsorbents for the treatment of wastewater containing organic pollutants (*e.g.*, synthetic dyes).

Acknowledgements

This research was funded by the Korea Ministry of Environment (The SEM projects; 2018002470005, South Korea) and the National Science Foundation (OIA-1632824, USA).

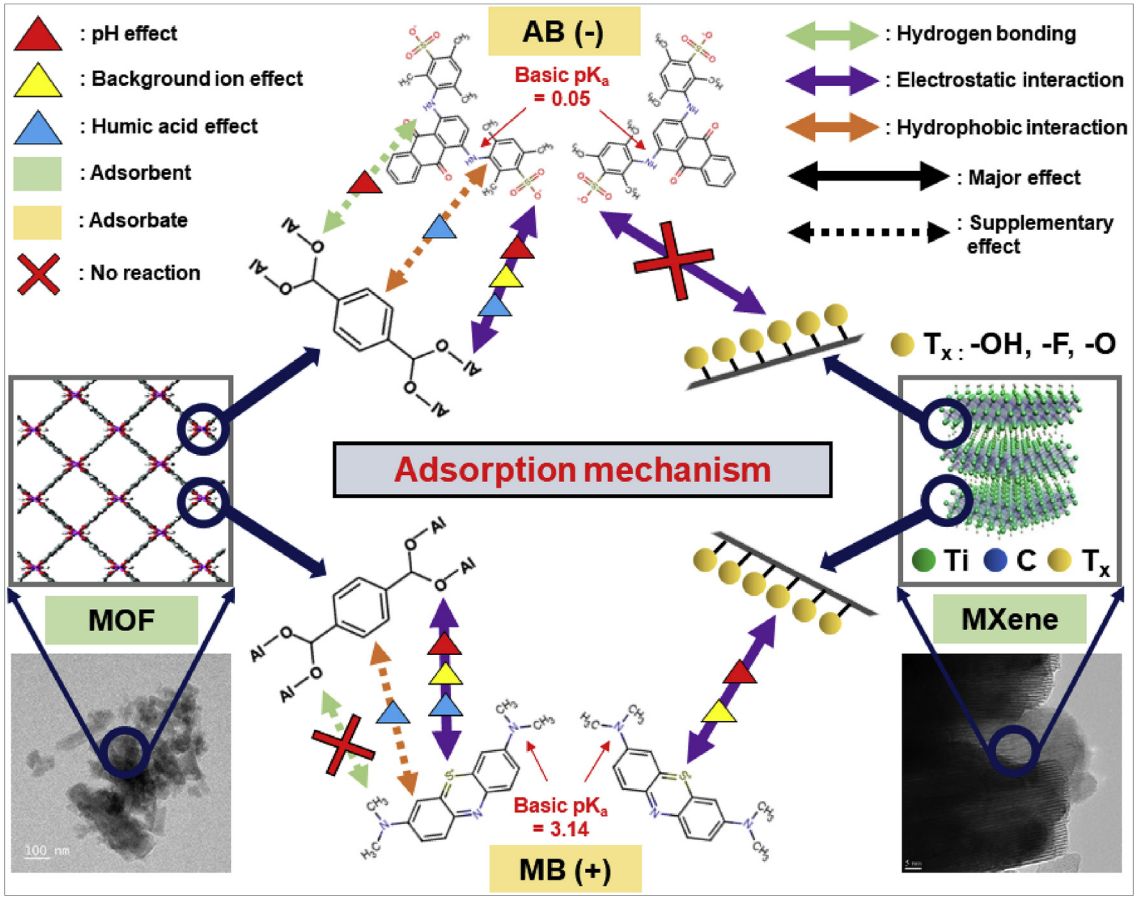

Fig. 5. Plausible schematic diagram for adsorption mechanisms of dyes by MXene and MOF.

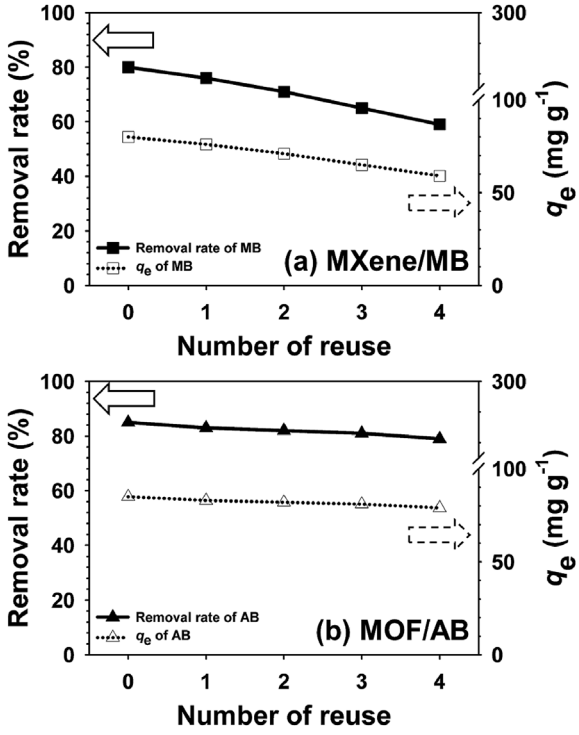

Fig. 6. Re-usability of MXene for MB and MOF for AB removal in four cycles of reuse.

Appendix A. Supplementary data

Supplementary data to this article can be found online at https://doi.org/10.1016/j.ceramint.2019.09.293.

References

[1] A.A. Alqadami, M. Naushad, Z.A. Alothman, T. Ahamad, Adsorptive performance of MOF nanocomposite for methylene blue and malachite green dyes: kinetics, isotherm and mechanism, J. Environ. Manag. 223 (2018) 29–36.
[2] E. Yılmaz, E. Sert, F.S. Atalay, Synthesis, characterization of a metal organic framework: MIL-53 (Fe) and adsorption mechanisms of methyl red onto MIL-53 (Fe), J. Taiwan Inst. Chem. E. 65 (2016) 323–330.
[3] A. Ayar, O. Gezici, M. Küçükosmanoğlu, Adsorptive removal of Methylene blue and Methyl orange from aqueous media by carboxylated diaminoethane sporopollenin: on the usability of an aminocarboxilic acid functionality-bearing solid-stationary phase in column techniques, J. Hazard Mater. 146 (2007) 186–193.
[4] S. Zhao, D. Chen, F. Wei, N. Chen, Z. Liang, Y. Luo, Removal of Congo red dye from aqueous solution with nickel-based metal-organic framework/graphene oxide composites prepared by ultrasonic wave-assisted ball milling, Ultrason. Sonochem. 39 (2017) 845–852.
[5] L. Joseph, B.-M. Jun, J.R.V. Flora, C.M. Park, Y. Yoon, Removal of heavy metals from water sources in the developing world using low-cost materials: a review, Chemosphere 229 (2019) 142–159.
[6] F. Meng, Z. Hong, J. Arndt, M. Li, M. Zhi, F. Yang, N. Wu, Visible light photocatalytic activity of nitrogen-doped $La_2Ti_2O_7$ nanosheets originating from band gap narrowing, Nano Res 5 (2012) 213–221.
[7] J. Guo, D. Jiang, Y. Wu, P. Zhou, Y. Lan, Degradation of methyl orange by Zn(0) assisted with silica gel, J. Hazard Mater. 194 (2011) 290–296.
[8] R.A. Pereira, M.F.R. Pereira, M.M. Alves, L. Pereira, Carbon based materials as novel redox mediators for dye wastewater biodegradation, Appl. Catal., B 144 (2014) 713–720.
[9] R. Qu, B. Xu, L. Meng, L. Wang, Z. Wang, Ozonation of indigo enhanced by carboxylated carbon nanotubes: performance optimization, degradation products, reaction mechanism and toxicity evaluation, Water Res. 68 (2015) 316–327.
[10] J. Han, B.-M. Jun, J. Heo, S. Kim, Y. Yoon, C.M. Park, Heterogeneous sonocatalytic degradation of an anionic dye in aqueous solution using a magnetic lanthanum dioxide carbonate-doped zinc ferrite-reduced graphene oxide nanostructure,

Ecotoxicol. Environ. Saf. 182 (2019) 109396–109404.
[11] A.N. Soon, B.H. Hameed, Heterogeneous catalytic treatment of synthetic dyes in aqueous media using Fenton and photo-assisted Fenton process, Desalination 269 (2011) 1–16.
[12] L. Xu, L.-S. Du, C. Wang, W. Xu, Nanofiltration coupled with electrolytic oxidation in treating simulated dye wastewater, J. Membr. Sci. 409–410 (2012) 329–334.
[13] S. Wang, Z.H. Zhu, Characterisation and environmental application of an Australian natural zeolite for basic dye removal from aqueous solution, J. Hazard Mater. 136 (2006) 946–952.
[14] M. Arami, N.Y. Limaee, N.M. Mahmoodi, N.S. Tabrizi, Removal of dyes from colored textile wastewater by orange peel adsorbent: equilibrium and kinetic studies, J. Colloid Interface Sci. 288 (2005) 371–376.
[15] E.T. Acar, S. Ortaboy, G. Atun, Adsorptive removal of thiazine dyes from aqueous solutions by oil shale and its oil processing residues: characterization, equilibrium, kinetics and modeling studies, Chem. Eng. J. 276 (2015) 340–348.
[16] Q. Qin, J. Ma, K. Liu, Adsorption of anionic dyes on ammonium-functionalized MCM-41, J. Hazard Mater. 162 (2009) 133–139.
[17] S.S. Tahir, N. Rauf, Removal of a cationic dye from aqueous solutions by adsorption onto bentonite clay, Chemosphere 63 (2006) 1842–1848.
[18] J. Saini, V.K. Garg, R.K. Gupta, N. Kataria, Removal of Orange G and Rhodamine B dyes from aqueous system using hydrothermally synthesized zinc oxide loaded activated carbon (ZnO-AC), J. Environ. Chem. Eng. 5 (2017) 884–892.
[19] Y.-H. Fan, S.-W. Zhang, S.-B. Qin, X.-S. Li, S.-H. Qi, An enhanced adsorption of organic dyes onto NH_2 functionalization titanium-based metal-organic frameworks and the mechanism investigation, Micropor. Mesopor. Mat. 263 (2018) 120–127.
[20] O. Mashtalir, K.M. Cook, V.N. Mochalin, M. Crowe, M.W. Barsoum, Y. Gogotsi, Dye adsorption and decomposition on two-dimensional titanium carbide in aqueous media, J. Mater. Chem. 2 (2014) 14334–14338.
[21] B.-M. Jun, S. Kim, J. Heo, N. Her, M. Jang, C.M. Park, Y. Yoon, Enhanced sono-catalytic degradation of carbamazepine and salicylic acid using a metal-organic framework, Ultrason. Sonochem. 56 (2019) 174–182.
[22] B.-M. Jun, S. Kim, J. Heo, C.M. Park, N. Her, M. Jang, Y. Huang, J. Han, Y. Yoon, Review of MXenes as new nanomaterials for energy storage/delivery and selected environmental applications, Nano Res 12 (2019) 471–487.
[23] A. Shahzad, M. Nawaz, M. Moztahida, J. Jang, K. Tahir, J. Kim, Y. Lim, V.S. Vassiliadis, S.H. Woo, D.S. Lee, $Ti_3C_2T_x$ MXene core-shell spheres for ultrahigh removal of mercuric ions, Chem. Eng. J. 368 (2019) 400–408.
[24] S. Li, L. Wang, J. Peng, M. Zhai, W. Shi, Efficient thorium(IV) removal by two-dimensional Ti_2CT_x MXene from aqueous solution, Chem. Eng. J. 366 (2019) 192–199.
[25] B.-M. Jun, S.H. Kim, S.K. Kwak, Y.-N. Kwon, Effect of acidic aqueous solution on chemical and physical properties of polyamide NF membranes, Appl. Surf. Sci. 444 (2018) 387–398.
[26] T.P.N. Nguyen, B.-M. Jun, Y.-N. Kwon, The chlorination mechanism of integrally asymmetric cellulose triacetate (CTA)-based and thin film composite polyamide-based forward osmosis membrane, J. Membr. Sci. 523 (2017) 111–121.
[27] B.-M. Jun, S. Kim, Y. Kim, N. Her, J. Heo, J. Han, M. Jang, C.M. Park, Y. Yoon, Comprehensive evaluation on removal of lead by graphene oxide and metal organic framework, Chemosphere 231 (2019) 82–92.
[28] B.-M. Jun, H.K. Lee, Y.-I. Park, Y.-N. Kwon, Degradation of full aromatic polyamide NF membrane by sulfuric acid and hydrogen halides: change of the surface/permeability properties, Polym. Degrad. Stab. 162 (2019) 1–11.
[29] B.-M. Jun, T.P.N. Nguyen, Y.-K. Kim, H.K. Lee, Y.-N. Kwon, Surface modification of TFC FO membrane using N-isopropylacrylamide (NIPAM) to enhance fouling resistance and cleaning efficiency, Desalin. Water Treat. 65 (2017) 11–21.
[30] S.-W. Han, W. Kim, Y. Lee, B.-M. Jun, Y.-N. Kwon, Investigation of Hydrate-induced Ice Desalination (HIID) and its application to a pretreatment of reverse osmosis (RO) process, Desalination 395 (2016) 8–16.
[31] G. Zou, J. Guo, Q. Peng, A. Zhou, Q. Zhang, B. Liu, Synthesis of urchin-like rutile titania carbon nanocomposites by iron-facilitated phase transformation of MXene for environmental remediation, J. Mater. Chem. 4 (2016) 489–499.
[32] A. Shahzad, K. Rasool, W. Miran, M. Nawaz, J. Jang, K.A. Mahmoud, D.S. Lee, Mercuric ion capturing by recoverable titanium carbide magnetic nanocomposite, J. Hazard Mater. 344 (2018) 811–818.
[33] Y. Lv, R. Zhang, S. Zeng, K. Liu, S. Huang, Y. Liu, P. Xu, C. Lin, Y. Cheng, M. Liu, Removal of p-arsanilic acid by an amino-functionalized indium-based metal–organic framework: adsorption behavior and synergetic mechanism, Chem. Eng. J. 339 (2018) 359–368.
[34] B.-M. Jun, H.K. Lee, Y.-N. Kwon, Acid-catalyzed hydrolysis of semi-aromatic polyamide NF membrane and its application to water softening and antibiotics enrichment, Chem. Eng. J. 332 (2018) 419–430.
[35] B.-M. Jun, T.P.N. Nguyen, S.-H. Ahn, I.-C. Kim, Y.-N. Kwon, The application of polyethyleneimine draw solution in a combined forward osmosis/nanofiltration system, J. Appl. Polym. Sci. 132 (2015) 42198–42206.
[36] M. Zhou, Y.-n. Wu, J. Qiao, J. Zhang, A. McDonald, G. Li, F. Li, The removal of bisphenol A from aqueous solutions by MIL-53(Al) and mesostructured MIL-53(Al), J. Colloid Interface Sci. 405 (2013) 157–163.
[37] Z. Hasan, S.H. Jhung, Removal of hazardous organics from water using metal-organic frameworks (MOFs): plausible mechanisms for selective adsorptions, J. Hazard Mater. 283 (2015) 329–339.
[38] A.K. Fard, G. McKay, R. Chamoun, T. Rhadfi, H. Preud'Homme, M.A. Atieh, Barium removal from synthetic natural and produced water using MXene as two dimensional (2-D) nanosheet adsorbent, Chem. Eng. J. 317 (2017) 331–342.
[39] Y. Gao, R. Kang, J. Xia, G. Yu, S. Deng, Understanding the adsorption of sulfonamide antibiotics on MIL-53s: metal dependence of breathing effect and adsorptive performance in aqueous solution, J. Colloid Interface Sci. 535 (2019) 159–168.
[40] K. Zhu, Y. Liu, J. Liu, A fast charging/discharging all-solid-state lithium ion battery based on PEO-MIL-53(Al)-LiTFSI thin film electrolyte, RSC Adv. 4 (2014) 42278–42284.
[41] A. Shahzad, K. Rasool, W. Miran, M. Nawaz, J. Jang, K.A. Mahmoud, D.S. Lee, Two-Dimensional $Ti_3C_2T_x$ MXene nanosheets for efficient copper removal from water, ACS Sustain. Chem. Eng. 5 (2017) 11481–11488.
[42] L. Joseph, B.-M. Jun, M. Jang, C.M. Park, J.C. Muñoz-Senmache, A.J. Hernández-Maldonado, A. Heyden, M. Yu, Y. Yoon, Removal of contaminants of emerging concern by metal-organic framework nanoadsorbents: a review, Chem. Eng. J. 369 (2019) 928–946.
[43] P. Gu, J. Xing, T. Wen, R. Zhang, J. Wang, G. Zhao, T. Hayat, Y. Ai, Z. Lin, X. Wang, Experimental and theoretical calculation investigation on efficient Pb(II) adsorption on etched Ti_3AlC_2 nanofibers and nanosheets, Environ. Sci. Nano 5 (2018) 946–955.
[44] C. Jung, J. Park, K.H. Lim, S. Park, J. Heo, N. Her, J. Oh, S. Yun, Y. Yoon, Adsorption of selected endocrine disrupting compounds and pharmaceuticals on activated biochars, J. Hazard Mater. 263 (2013) 702–710.
[45] C.M. Park, J. Han, K.H. Chu, Y.A.J. Al-Hamadani, N. Her, J. Heo, Y. Yoon, Influence of solution pH, ionic strength, and humic acid on cadmium adsorption onto activated biochar: experiment and modeling, J. Ind. Eng. Chem. 48 (2017) 186–193.
[46] K.T. Wong, Y. Yoon, S.A. Snyder, M. Jang, Phenyl-functionalized magnetic palm-based powdered activated carbon for the effective removal of selected pharmaceutical and endocrine-disruptive compounds, Chemosphere 152 (2016) 71–80.
[47] B.-M. Jun, H.S. Hwang, J. Heo, J. Han, M. Jang, J. Sohn, C.M. Park, Y. Yoon, Removal of selected endocrine-disrupting compounds using Al-based metal organic framework: performance and mechanism of competitive adsorption, J. Ind. Eng. Chem. 79 (2019) 345–352 in press.
[48] B.-M. Jun, J. Heo, C.M. Park, Y. Yoon, Comprehensive evaluation of the removal mechanism of carbamazepine and ibuprofen by metal organic framework, Chemosphere 235 (2019) 527–537.
[49] A. Batra, G. Kladnik, H. Vázquez, J.S. Meisner, L. Floreano, C. Nuckolls, D. Cvetko, A. Morgante, L. Venkataraman, Quantifying through-space charge transfer dynamics in π-coupled molecular systems, Nat. Commun. 3 (2012) 1086–1101.
[50] J. Han, B.-M. Jun, J. Heo, G. Lee, Y. Yoon, C.M. Park, Highly efficient organic dye removal from waters by magnetically recoverable $La_2O_2CO_3/ZnFe_2O_4$-reduced graphene oxide nanohybrid, Ceram. Int. 45 (2019) 19247–19256.